ANALYTICAL MODELING OF CIRCULAR GLARE LAMINATED PLATES UNDER LATERAL INDENTATION

George J. Tsamasphyros and George S. Bikakis

Strength of Materials Laboratory, National Technical University of Athens,
9 Iroon Polytechniou, Zographou, GR 157 73, Athens, Greece

Received 16 December 2008; accepted 7 April 2009

ABSTRACT

In this paper analytical solutions are derived to predict the static response of thin circular clamped GLARE fibre-metal laminated plates under the action of a lateral hemispherical indentor. The load-indentation curve is calculated along with the first failure load and deflection due to glass-epoxy tensile fracture. The Ritz method is employed with one, two and three-parameter Ritz approximation functions. The derived formulas are applied to GLARE 2-2/1-0.3 and to GLARE 3-3/2-0.4 circular plates with various diameters. The results converge satisfactorily in all examined cases. The calculated load-indentation curve and the first failure agree well with published experimental data for the case of a GLARE 2-2/1-0.3 plate with a radius of 40 mm (failure load within 7% and failure deflection within 3%). The same load-indentation curves are also calculated using ANSYS and by comparison to FEM results the validity of the analytical model is further verified. No analytical solution of this problem is known to the authors.

Keywords: GLARE, load-indentation response, tensile fracture.

1. INTRODUCTION

GLARE is a Fibre-Metal Laminated material used in aerospace structures which are frequently subjected to various impact damages [1-5]. A high percentage of the total energy absorbed by GLARE plates during impacts is due to the static deformation of the plate [1, 6-7]. Hence, response of GLARE plates subjected to lateral indentation is very important as far as their overall impact behaviour is concerned.

This paper deals with the static response of thin circular clamped GLARE fibre-metal laminated plates under the action of a lateral hemispherical indentor located at the centre of the plate. In reference [1] Vlot used an elastic-plastic impact model to solve this problem numerically assuming a deformation profile based on experimental data. Hoo Fatt et al. [6] used the principle of minimum potential energy to model analytically the response of fully clamped square GLARE panels assuming a deformation profile which resembles that of a stretched membrane. They also calculated the first failure load due to glass-epoxy tensile fracture.

The objective of this paper is to develop an analytical model for the calculation of static load-indentation curve and the first failure due to glass-epoxy tensile fracture applicable to circular plates. The Ritz method is employed in order to solve the problem in association with suitable approximation functions. Formulas corresponding to one, two and three-parameter Ritz approximations have been derived. These formulas provide a means to verify the convergence of the results when applied for a specific GLARE grade. In this work the load-indentation curve and the first failure are calculated applying the derived formulas to GLARE 2-2/1-0.3 and to GLARE 3-3/2-0.4 plates with various diameters and the results converge satisfactorily in all examined cases. For the case of a GLARE 2-2/1-0.3 plate with a radius of 40 mm, the results are in good agreement with experimental data from reference [1]. The same load-indentation curves are also calculated using ANSYS and by comparison to FEM results the validity of our analytical model is further verified. No analytical solution of this problem is known to the authors.

2. PROBLEM DEFINITION

We consider a thin clamped circular GLARE plate with radius α and thickness t as shown in Fig. 1. The plate is loaded statically by an indentor with a hemispherical tip of radius R acting at the centre. The plate consists of alternating layers of aluminum and

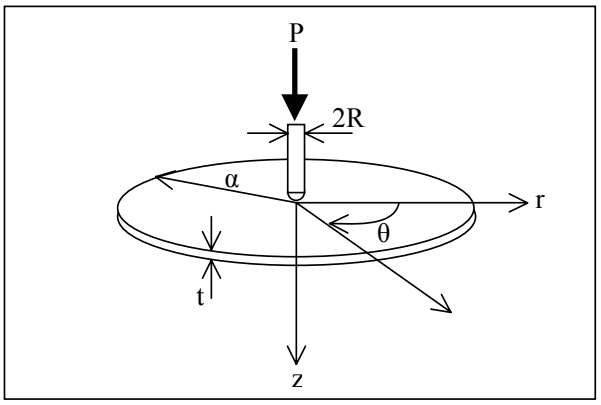

Fig. 1 Circular plate problem geometry and coordinate system

glass-epoxy. The aspect ratio α/t is assumed very high so that shear deformation and local indentation are negligible.

A polar coordinate system (r,θ,z) with the origin at the centre of the plate is employed as illustrated in Fig. 1. The lateral displacements, w, of the plate satisfy the following boundary conditions:

$$w = 0 \qquad (r = \alpha) \tag{1}$$

$$\frac{\partial w}{\partial r} = 0 \qquad (r = \alpha) \tag{2}$$

As the indentor progresses the load P applied on the plate and the corresponding central deflection wo increase. We will derive analytical expressions for the calculation of the (P , w_o) curve. We will also calculate the first failure load and deflection due to glass-epoxy tensile fracture.

3. ANALYSIS

In order to obtain analytical expressions for the load-indentation curve we idealize the material behaviour of aluminum as rigid-perfectly plastic and the unidirectional glass-epoxy as linear elastic. We assume stress distributions corresponding to fully plastic bending and membrane states for aluminum layers. This assumption was also made for the stresses in reference [6]. From the experimental data in reference [1] it is concluded that GLARE plates will undergo very large deflections, several times the plate thickness, before tensile fracture of glass-epoxy occurs. Although bending resistance governs the plate's response for small deflections, membrane resistance plays the governing role when deflections become large as referred also in [7, 8]. Furthermore, in the case of very thin plates that may have deflections many times larger than their thickness, the resistance of the plate to bending can be neglected. We will first consider the case of membrane only resistance and then the case of both bending and membrane resistance of the GLARE plates.

3.1. Strain Energy Equations

We assume that deflections are large, in-plane deformations are negligible compared with the transverse deflections and that the strains are finite. The Cartesian strain components for large deflections of plates and negligible in-plane deformations are given by:

$$\varepsilon_x = \frac{1}{2}\left(\frac{\partial w}{\partial x}\right)^2, \quad \varepsilon_y = \frac{1}{2}\left(\frac{\partial w}{\partial y}\right)^2, \quad \gamma_{xy} = \frac{\partial w}{\partial x}\frac{\partial w}{\partial y} \tag{3}$$

The membrane strain energy of the plate is [8]:

$$U_m = \frac{1}{2}\iint_T \left(N_x\varepsilon_x + N_y\varepsilon_y + N_{xy}\gamma_{xy}\right)dxdy \tag{4}$$

where N_x, N_y and N_{xy} are the in-plane forces acting on the plate and T is the integration domain defined by the plate's boundary. The assumed stress distribution corresponds to the fully plastic membrane state and leads to the following expressions for the in-plane forces of the aluminum layers:

$$N_x = N_y = m\sigma_o t_{Al}, \qquad N_{xy} = m\frac{\sigma_o}{\sqrt{3}}t_{Al} \tag{5}$$

where m is the number of aluminum layers, σ_o is the yield stress of aluminum and t_{Al} is the thickness of each aluminum layer.

Static indentations tests presented in reference [1] revealed that during loading the fibre-metal laminates have a virtually axisymmetrical deflection shape. Such a deflection shape was employed by Vlot for his elastic-plastic impact model. We will consider axisymmetrical deflection shape so that:

$$\frac{\partial w}{\partial x} = \frac{\partial w}{\partial r}\cos\theta, \qquad \frac{\partial w}{\partial y} = \frac{\partial w}{\partial r}\sin\theta, \tag{6}$$

In order to obtain an expression for the membrane strain energy of aluminum layers we take into account that N_x, N_y and N_{xy} do not depend on (x,y) coordinates. Substitution of equations (3) in equation

(4) and transformation in polar coordinates using expressions (6) yields:

$$U_m^{Al} = \frac{N_x}{4}\iint_T\left(\frac{\partial w}{\partial r}\cos\theta\right)^2 rdrd\theta + \frac{N_y}{4}\iint_T\left(\frac{\partial w}{\partial r}\sin\theta\right)^2 rdrd\theta + \frac{N_{xy}}{2}\iint_T\left(\frac{\partial w}{\partial r}\right)^2 \cos\theta\sin\theta rdrd\theta \quad (7)$$

For a symmetric laminate with specially orthotropic layers the in-plane forces are [9]:

$$N_x = A_{11}\varepsilon_x + A_{12}\varepsilon_y, \quad N_y = A_{12}\varepsilon_x + A_{22}\varepsilon_y, \quad N_{xy} = A_{66}\gamma_{xy} \quad (8)$$

where A_{ij} are the extensional stiffnesses of the laminate. Substitution of equations (3) and (8) into equation (4) yields the following expression for the membrane strain energy of the prepreg layers:

$$U_m^{Pre} = \frac{1}{8}\iint_T\left[A_{11}\left(\frac{\partial w}{\partial x}\right)^4 + A_{22}\left(\frac{\partial w}{\partial y}\right)^4 + \left(2A_{12}+4A_{66}\right)\left(\frac{\partial w}{\partial x}\right)^2\left(\frac{\partial w}{\partial y}\right)^2\right]dxdy \quad (9)$$

Since A_{ij} do not depend on (x,y) coordinates, equation (9) is transformed in polar coordinates using expressions (6) as follows:

$$U_m^{Pre} = \frac{A_{11}}{8}\iint_T\left(\frac{\partial w}{\partial r}\cos\theta\right)^4 rdrd\theta + \frac{A_{22}}{8}\iint_T\left(\frac{\partial w}{\partial r}\sin\theta\right)^4 rdrd\theta + \frac{A_{12}+2A_{66}}{4}\iint_T\left(\frac{\partial w}{\partial r}\right)^4 \cos^2\theta\sin^2\theta rdrd\theta \quad (10)$$

The bending strain energy of the plate is [10]:

$$U_b = \frac{1}{2}\iint_T\left(M_x\frac{\partial^2 w}{\partial x^2} + M_y\frac{\partial^2 w}{\partial y^2} + 2M_{xy}\frac{\partial^2 w}{\partial x\partial y}\right)dxdy \quad (11)$$

where M_x, M_y and M_{xy} are the bending and twisting moments acting on the plate. The assumed stress distribution corresponds to the fully plastic bending state and leads to the following expressions for the moments of the aluminum layers (for *m=1* or *m=2,4...* or *m=3,5...* respectively in equation 12):

$$M_x = \sigma_o\frac{t_{Al}^2}{4}, \quad M_x = \sigma_o t_{Al}\sum_{i=1}^{m} Z_i, \quad M_x = \sigma_o t_{Al}\sum_{i=1}^{m-1} Z_i + \sigma_o\frac{t_{Al}^2}{4} \quad (12)$$

$$M_x = M_y \qquad M_{xy} = \frac{M_x}{\sqrt{3}} \quad (13)$$

where Z_i is the geometric distance of each aluminum layer from the neutral surface of the plate.

In order to transform equation (11) in polar coordinates, we use the following expressions:

$$\frac{\partial^2 w}{\partial x^2} = \frac{\partial^2 w}{\partial r^2}\cos^2\theta + \frac{\partial w}{\partial r}\frac{\sin^2\theta}{r}, \qquad \frac{\partial^2 w}{\partial y^2} = \frac{\partial^2 w}{\partial r^2}\sin^2\theta + \frac{\partial w}{\partial r}\frac{\cos^2\theta}{r}$$
$$\frac{\partial^2 w}{\partial x\partial y} = \frac{\partial^2 w}{\partial r^2}\sin\theta\cos\theta - \frac{\partial w}{\partial r}\frac{\sin\theta\cos\theta}{r} \quad (14)$$

In order to obtain an expression for the bending strain energy of aluminum layers we take into account that M_x, M_y and M_{xy} do not depend on (x,y) coordinates. Transformation of equation (11) in polar coordinates using expressions (14) yields:

$$U_b^{Al} = \frac{M_x}{2}\iint_T\left(\frac{\partial^2 w}{\partial r^2}\cos^2\theta + \frac{\partial w}{\partial r}\frac{\sin^2\theta}{r}\right)rdrd\theta + \frac{M_y}{2}\iint_T\left(\frac{\partial^2 w}{\partial r^2}\sin^2\theta + \frac{\partial w}{\partial r}\frac{\cos^2\theta}{r}\right)rdrd\theta + M_{xy}\iint_T\left(\frac{\partial^2 w}{\partial r^2}\sin\theta\cos\theta - \frac{\partial w}{\partial r}\frac{\sin\theta\cos\theta}{r}\right)rdrd\theta \quad (15)$$

For a symmetric laminate with specially orthotropic layers the moments are [9]:

$$M_x = D_{11}\frac{\partial^2 w}{\partial x^2} + D_{12}\frac{\partial^2 w}{\partial y^2}, \quad M_y = D_{12}\frac{\partial^2 w}{\partial x^2} + D_{22}\frac{\partial^2 w}{\partial y^2}, \quad M_{xy} = 2D_{66}\frac{\partial^2 w}{\partial x\partial y} \quad (16)$$

where D_{ij} are the bending stiffnesses of the laminate. Since D_{ij} do not depend on (x,y) coordinates, equation (11) is transformed in polar coordinates using expressions (14) and (16) as follows:

$$U_b^{Pre} = \frac{D_{11}}{2}\iint_T\left(\frac{\partial^2 w}{\partial r^2}\cos^2\theta + \frac{\partial w}{\partial r}\frac{\sin^2\theta}{r}\right)^2 rdrd\theta + \frac{D_{22}}{2}\iint_T\left(\frac{\partial^2 w}{\partial r^2}\sin^2\theta + \frac{\partial w}{\partial r}\frac{\cos^2\theta}{r}\right)^2 rdrd\theta + D_{12}\iint_T\left(\frac{\partial^2 w}{\partial r^2}\cos^2\theta + \frac{\partial w}{\partial r}\frac{\sin^2\theta}{r}\right)\left(\frac{\partial^2 w}{\partial r^2}\sin^2\theta + \frac{\partial w}{\partial r}\frac{\cos^2\theta}{r}\right)rdrd\theta + 2D_{66}\iint_T\left(\frac{\partial^2 w}{\partial r^2}\sin\theta\cos\theta - \frac{\partial w}{\partial r}\frac{\sin\theta\cos\theta}{r}\right)^2 rdrd\theta \quad (17)$$

3.2. Ritz Method Application

We consider the following approximation function for the deformation profile of the plate which satisfies boundary conditions (1) and (2):

$$w_i(r) = \sum_{j=1}^{i}\lambda_j\left(1-\sin\frac{(4j-3)\pi r}{2\alpha}\right), \quad 0\le r\le\alpha, \quad i=1,2,3,... \quad (18)$$

where λ_j are the Ritz coefficients. This deformation profile has not zero slope at the centre of the plate. It is noted that the same boundary conditions and non zero slope at the centre are satisfied by the experimental deformation profile employed by Vlot in reference [1].

Using the above deformation profile strain energy components can be calculated from equations (7), (10), (15) and (17). As already mentioned, we consider the case of membrane only resistance and the case of both bending and membrane resistance by adding the membrane only and both bending and membrane components for the calculation of the total strain energy U.

The total potential energy functional is:

$$\Pi = U - Pw_o \tag{19}$$

where Pwo is the work done by the indentation load. From equation (18) we have:

$$w_i(0) = w_o = \sum_{j=1}^{i} \lambda_j , \qquad i = 1,2,3,... \tag{20}$$

Minimization of the functional Π yields:

$$\frac{\partial U}{\partial \lambda_j} = P , \qquad j = 1,2,3,...,i \tag{21}$$

Equation (21) gives an (*ixi*) non-linear system of algebraic equations from which the Ritz coefficients λ_j can be determined for each specific value of load *P*. Substitution of λ_j into equation (20) gives the corresponding value of wo. In this way (P , w_o) curve can be calculated. Obviously, for *i*=1 an algebraic expression of *P* as a function of w_o is directly obtained. In appendix A we present the derived formulas corresponding to one, two and three-parameter Ritz approximations.

3.3. Glass-Epoxy Tensile Fracture

We follow the reasoning of reference [6]. First failure would occur when the tensile strain in the glass-epoxy reaches the tensile failure strain ε_{crit}. Since deflections are very large, we ignore bending strains and assume that all glass-epoxy layers break at the same time when the membrane strain reaches the limit value of the prepreg. The radial membrane strain ε_r in the plate is given by:

$$\varepsilon_r = \frac{1}{2}\left(\frac{\partial w}{\partial r}\right)^2 \tag{22}$$

The maximum value of ε_r, for *r*=0, is obtained by combination of equations (18) and (22):

$$\varepsilon_{r\max} = \frac{1}{2}\sum_{j=1}^{i}\left(\frac{\lambda_j(4j-3)\pi}{2a}\right)^2 , \qquad i = 1,2,3,... \tag{23}$$

Glass-epoxy tensile fracture occurs when $\varepsilon_{r\max} = \varepsilon_{crit}$, or equivalently, when:

$$\sum_{j=1}^{i} \lambda_j(4j-3) = \frac{2\alpha}{\pi}\sqrt{2\varepsilon_{crit}} , \qquad i = 1,2,3,... \tag{24}$$

Using equations (21), we start increasing the indentation load *P*, until the corresponding values of λ_j satisfy condition (24). When this happens, the indentation load P has reached the critical value P_{crit} and the corresponding first failure displacement w_{ocrit} is then calculated from equation (20) for those λ_j values.

For *i*=1, equation (20) gives $w_{ocrit}=\lambda_1$ and w_{ocrit} is directly obtained from equation (24), while the corresponding P_{crit} is calculated by substituting w_{ocrit} to equation (21).

4. RESULTS

We apply the derived formulas in order to calculate the load-indentation curve and the first failure of GLARE 2-2/1-0.3 plates. GLARE 2-2/1-0.3 fibre-metal laminate consists of two external 2024-T3 aluminum layers and two R-glass UD fibre prepregs in the middle. Each aluminum layer has a thickness of 0.3 mm and each prepreg has a thickness of 0.1 mm. Prepregs have the same orientation. The material properties considered for our calculations are given in Table 1. All available properties of reference [1] have been used. Remaining material properties have been taken from reference [6] apart from v_{21} which has been calculated based on the reciprocal relations.

We also apply the derived formulas in order to calculate the load-indentation curve and the first failure of GLARE 3-3/2-0.4 plates. GLARE 3-3/2-0.4 fibre-metal laminate consists of the following lay-up:

[2024-T3 / 0^0 glass / 90^0 glass / 2024-T3 / 90^0 glass / 0^0 glass / 2024-T3]

Each 2024-T3 aluminum layer has a thickness of

,

Table 1: GLARE 2-2/1-0.3 material properties.

$E_{11} = 47.3$ GPa (long. prepreg stiffness)	$v_{12} = 0.25$ (prepreg Poisson's ratio)
$E_{22} = 17$ GPa (transverse prepreg stiffness)	$\varepsilon_{crit} = 0.055$ (prepreg tensile failure strain)
$G_{12} = 7$ GPa (prepreg shear modulus)	$\sigma_o = 340$ MPa (aluminum yield strength)

0.4 mm. Each prepreg ply has a thickness of 0.125 mm and consists of S2-glass UD fibre prepregs. The material properties considered for our calculations are those given in Table 1, apart from εcrit which, according to our correspondence with the manufacturer of GLARE 3, is equal to 0.047.

In Figs 2 and 3 the static (P, w_o) curves corresponding to the membrane strain energy of a GLARE 2-2/1-0.3 plate with 40 mm radius and of a GLARE 3-3/2-0.4 plate with 75 mm radius are depicted. In Fig.s 4 and 5 the static (P, w_o) curves corresponding to both bending and membrane strain energy are depicted for the same GLARE plates. Each curve stops at the point of the predicted first failure. It can be seen that the results have converged satisfactorily in all cases. It is noted that the rigid-perfectly plastic assumption for the aluminum yields the existence of constant bending terms in (P, w_o) expressions. Due to these terms the plate does not deflect until the load reaches a finite value that causes plastic flow. This is clearly illustrated in Fig.s 4 and 5. In Fig. s 6 and 7 the three-parameter membrane only and both membrane and bending (P, w_o) curves are compared for the aforementioned GLARE plates. The expected small contribution of bending stiffness in comparison with the membrane stiffness to the response of the plate can be observed.

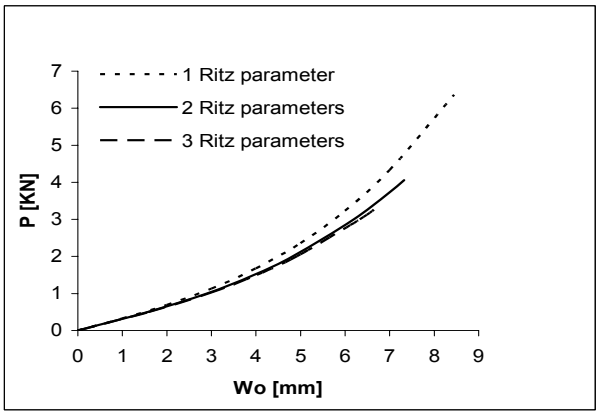

Fig. 2: Membrane load-indentation curves for GLARE 2 plate with 40 mm radius

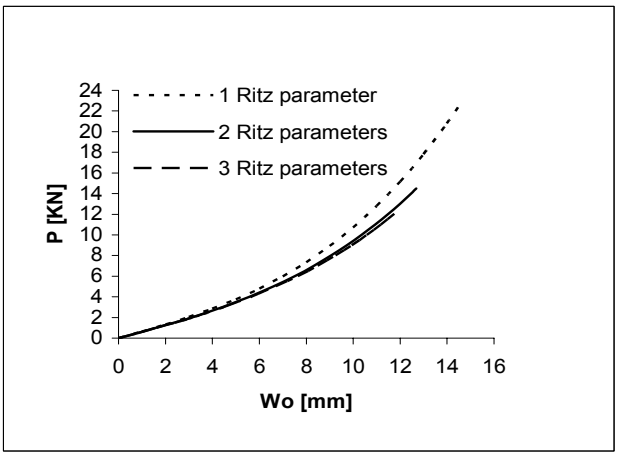

Fig. 3: Membrane load-indentation curves for GLARE 3 plate with 75 mm radius

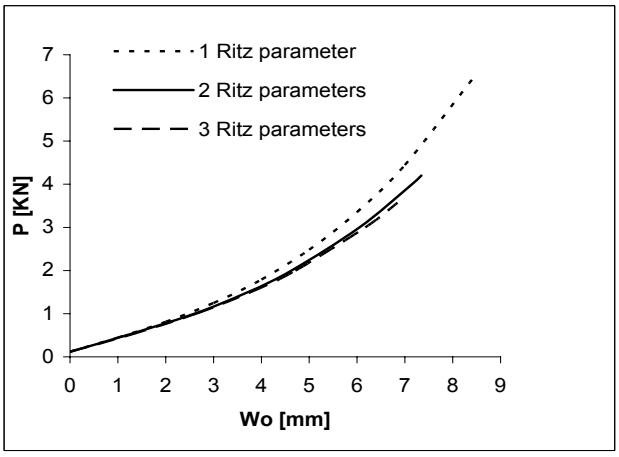

Fig. 4: Membrane and Bending load-indentation curves for GLARE 2 plate with 40 mm radius

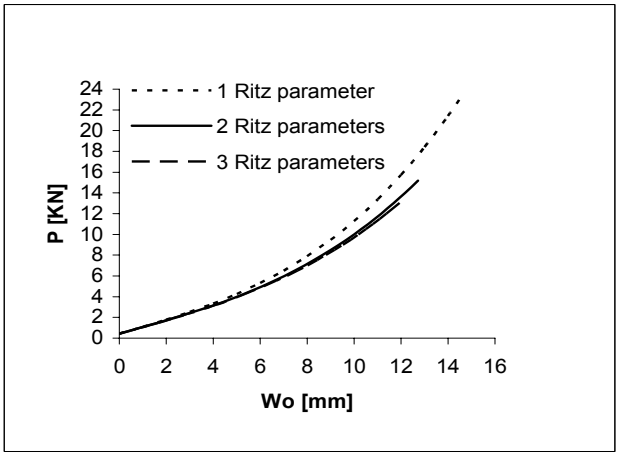

Fig. 5: Membrane and Bending load-indentation curves for GLARE 3 plate with 75 mm radius

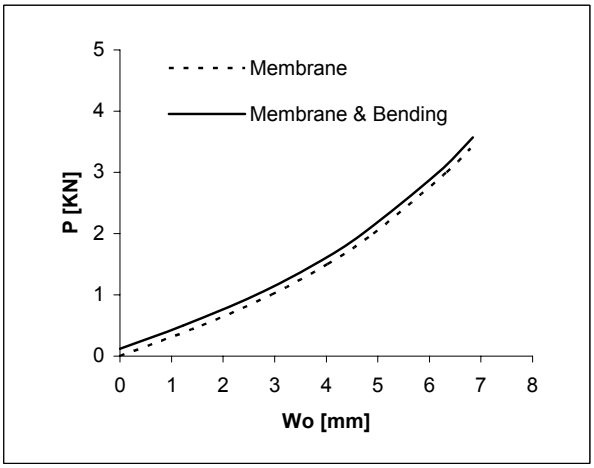

Fig. 6: Three Ritz parameters load-indentation curves for GLARE 2 plate with 40 mm radius

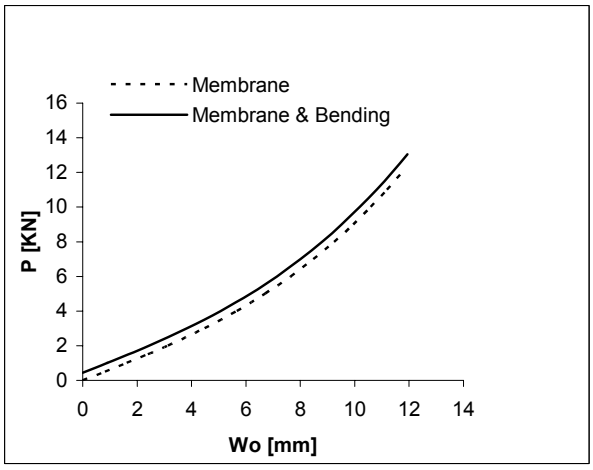

Fig. 7: Three Ritz parameters load-indentation curves for GLARE 3 plate with 75 mm radius

We have also calculated the (P, w_o) curves of GLARE 2-2/1-0.3 plates with 35 mm and 45 mm radius and of GLARE 3-3/2-0.4 plates with 65 mm and 70 mm radius. The obtained results lead to the same conclusions. By careful examination of all results we have obtained, it is concluded that the (P, w_o) curve of a GLARE plate under lateral indentation can be well approximated up to the point of first failure, considering only one Ritz parameter and only the membrane components of the strain energy. This conclusion is very useful in cases where the prediction of first failure is not mandatory, since it reduces the required calculations dramatically.

5. COMPARISON WITH EXPERIMENT AND FEM RESULTS

In reference [1], an experimental (P, w_o) curve is published for a GLARE 2-2/1-0.3 plate with 40 mm radius. In Fig. 8, the analytically calculated three-parameter (P, w_o) curves corresponding to the membrane strain energy only and to both bending and membrane strain energy of a GLARE 2-2/1-0.3 plate with 40 mm radius are compared with the above experimental curve. Both analytical and experimental curves stop at the point of the predicted first failure. The good agreement of analytical calculations with the experimental data is illustrated in Fig. 8. The predicted first failure load and deflection compare well with their experimental values from reference [1]. The best prediction (failure load within 7% and failure deflection within 3%) corresponds to the three-parameter Ritz approximation that takes into account both bending and membrane stiffness of the plate.

In order to further verify the validity of our analytical model, we implement a 3-D solid modelling procedure with ANSYS. We employ an isotropic non-linear elastoplastic material model which obeys a true stress-strain relation for aluminum. An orthotropic linear elastic material model is used for the glass-epoxy. The contact between the indentor and the plate is simulated by contact elements. We use non-linear analysis with geometric and material non-linearities. The indentor is forced to move and deform the plate incrementally. Analysis stops when first failure due to glass-epoxy tensile fracture occurs. The convergence of FEM results is checked by implementing models with increasing mesh density. This FEM procedure is applied to GLARE 2-2/1-0.3 plates with 35 mm, 40 mm and 45 mm radius and to GLARE 3-3/2-0.4 plates with 65 mm, 70 mm and 75 mm radius. In Fig. 8, the numerically calculated (P, w_o) curve is compared with the corresponding experimental curve. Both numerical and experimental curves stop at the point of the predicted first failure. The close agreement of FEM calculations with the experimental data is illustrated in Fig. 8. The numerically predicted first failure load and deflection compare well with their experimental values from reference [1] (failure load within 2% and failure deflection within 5%).

In Figs 8 and 9 the analytically calculated three-pa-

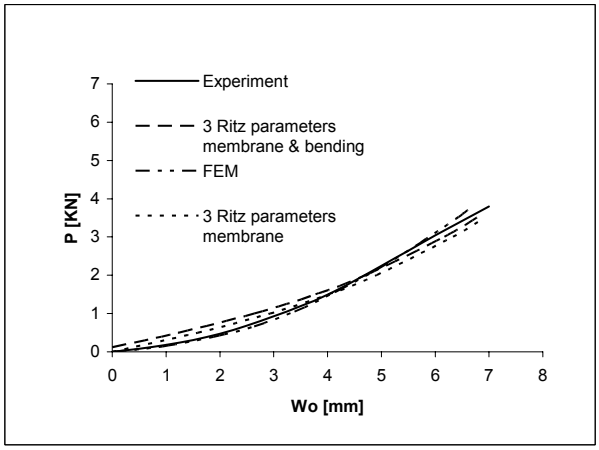

Fig. 8: Experimental versus calculated load-indentation curves for GLARE 2 plate with 40 mm radius

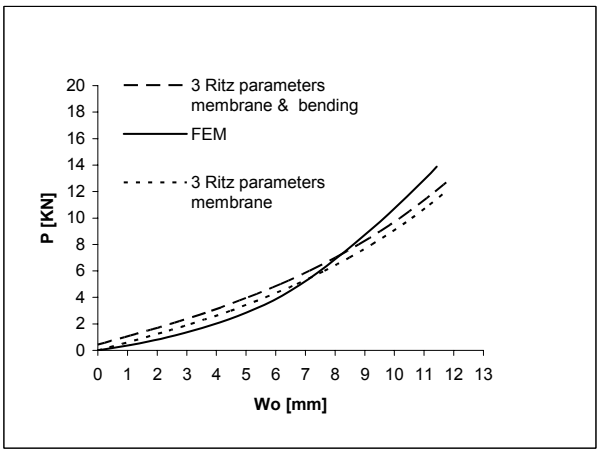

Fig. 9: Analytical versus numerical load-indentation curves for GLARE 3 plate with 75 mm radius

rameter (P , w_o) curves corresponding to the membrane strain energy only and to both bending and membrane strain energy of a GLARE 2-2/1-0.3 plate with 40 mm radius and of a GLARE 3-3/2-0.4 plate with 75 mm radius are compared with the corresponding numerical curves. Both analytical and numerical curves stop at the point of the predicted first failure.

The good agreement between analytical and FEM calculations is illustrated in Fig.s 8 and 9. The analytically predicted first failure load and deflection compare well with their numerical values from ANSYS. The best prediction (failure load within 5% and 6% , failure deflection within 3% and 5%) corresponds to the three-parameter Ritz approximation that takes into account both bending and membrane stiffness of the plate. A good agreement between analytical and FEM calculations has also been found for the cases of GLARE 2-2/1-0.3 plates with 35 mm and 45 mm radius and of GLARE 3-3/2-0.4 plates with 65 mm and 70 mm radius.

6. CONCLUSIONS

In this work we have developed an analytical model for the prediction of the static load-indentation curve of thin circular clamped GLARE fibre-metal laminated plates that deflect under the action of a lateral hemispherical indentor located at their centre. The model also predicts the first failure load and deflection due to the glass-epoxy tensile fracture.

The model is used to predict the response of circular GLARE 2-2/1-0.3 plates with 35 mm, 40 mm and 45 mm radius and the response of circular GLARE 3-3/2-0.4 plates with 65 mm, 70 mm and 75 mm radius. The results based on the three-parameter Ritz approximation functions converge satisfactorily in all examined cases. Also, the expected governing role of the membrane in comparison with the bending stiffness for these problems is found. For the case of a circular GLARE 2-2/1-0.3 plate with 40 mm radius, the predicted static load-indentation curve agrees well with the corresponding experimental curve. The first failure load and deflection are within 7% and 3% of their experimental values respectively.

For all of the examined cases, the analytically calculated static load-indentation curves and first failures agree well with the corresponding numerical results calculated with FEM using ANSYS. In this regard, we further verify the validity of our analytical model. The validity of our FEM modelling procedure is also demonstrated by the close agreement between numerical results and the aforementioned experimental data for the case of a circular GLARE 2-2/1-0.3 plate with 40 mm radius.

Our analytical model can be used for the design of circular GLARE plates under lateral indentation and for the evaluation of the impact properties of different GLARE grades. Furthermore, this analytical model is expected to predict satisfactorily the lateral indentation response of circular plates consisting of

other advanced hybrid material systems of alternating metal layers bonded to fibre-reinforced polymer layers, provided that our assumptions remain valid.

References:

1. **Vlot, A.,** "Impact loading on fibre metal laminates", *Int. J. Impact Engng.,* 18/3 (1996), 291-307.
2. **Vlot, A.,** "Impact properties of fibre metal laminates", *Compos. Eng.,* 3/10 (1993), 911-927.
3. **Laliberte, J.F., Poon, C., Straznicky, P.V., Fahr, A.,** "Post-impact fatigue damage growth in fibre-metal laminates", *Int. J. Fatigue.,* 24 (2002), 249-255.
4. **Vogelesang, L.B., Vlot, A.,** "Development of fibre metal laminates for advanced aerospace structures", *J. Mater. Process. Tech.,* 103 (2000), 1-5.
5. **Vermeeren, C.A.J.R.,** "An historic overview of the development of fibre metal laminates", *Appl. Compos. Mater.,* 10 (2003), 189-205.
6. **Hoo Fatt, M.S., Lin, C., Revilock Jr., D.M., Hopkins, D.A.,** "Ballistic impact of GLARETM fibre-metal laminates", *Comp. Struct.,* 61/1-2 (2003) 73-88.
7. **Lin, C., Hoo Fatt, M.S.,** "Perforation of composite plates and sandwich panels under quasi-static and projectile loading", *J. Comp. Mater.,* 40/20 (2006), 1801-1840.
8. **Timoshenko, S.P., Woinowsky-Krieger, S.,** *Theory of plates and shells,* McGraw-Hill, Singapore, 1959.
9. **Jones, R.M.,** *Mechanics of composite materials,* Taylor & Francis, Philadelphia, 1999.
10. **Ugural, A.C.,** *Stresses in plates and shells,* McGraw-Hill, Singapore, 1999.

APPENDIX A. ONE, TWO AND THREE-PARAMETER RITZ APPROXIMATIONS

For *i*=1, considering both bending and membrane components of strain energy we obtain the following expression:

$$P=\left[0.576\left(N_x+N_y\right)+0.734N_{xy}\right]w_o+\left[0.62\left(A_{11}+A_{22}\right)+\right.$$
$$\left.+0.412\left(A_{12}+2A_{66}\right)\right]\frac{w_o^3}{\alpha^2}+4M_{xy}+ \quad (25)$$
$$+\left[\left(3.318+2.906\ln\alpha\right)\left(D_{11}+D_{22}\right)+\left(-8.124+1.938\ln\alpha\right)D_{12}+\right.$$
$$\left.+\left(14.758+3.876\ln\alpha\right)D_{66}\right]\frac{w_o}{\alpha^2}$$

For *i*=1, considering only the membrane components of strain energy, *P* is calculated from expression (25) where M_{xy} and all D_{ij} terms are now equal to zero.

For *i*=2, considering both bending and membrane components of strain energy we obtain the following (2x2) non-linear system of algebraic equations, from which λ_1 and λ_2 can be determined for specific values of load *P*:

$$P=2N_1\lambda_1-N_3\lambda_2+4M_1\lambda_1^3-M_5\lambda_2^3+$$
$$+2M_3\lambda_1\lambda_2^2-3M_4\lambda_1^2\lambda_2+4M_{xy}+2C_1\lambda_1+C_3\lambda_2 \quad (26)$$
$$P=-N_3\lambda_1+2N_2\lambda_2-M_4\lambda_1^3+4M_2\lambda_2^3-3M_5\lambda_1\lambda_2^2+$$
$$+2M_3\lambda_1^2\lambda_2+4M_{xy}+2C_2\lambda_2+C_3\lambda_1 \quad (27)$$

where:

$$N_1=0.288(N_x+N_y)+0.367N_{xy},$$
$$N_2=11.916(N_x+N_y)+15.171N_{xy}, \quad (28)$$
$$N_3=0.218(N_x+N_y)+0.278N_{xy}$$

$$M_1=\left[0.155(A_{11}+A_{22})+0.103\left(A_{12}+2A_{66}\right)\right]\frac{1}{\alpha^2},$$
$$M_2=\left[205.585(A_{11}+A_{22})+137.056\left(A_{12}+2A_{66}\right)\right]\frac{1}{\alpha^2} \quad (29)$$

$$M_3=\left[19.449(A_{11}+A_{22})+12.966\left(A_{12}+2A_{66}\right)\right]\frac{1}{\alpha^2},$$
$$M_4=\left[1.211(A_{11}+A_{22})+0.807\left(A_{12}+2A_{66}\right)\right]\frac{1}{\alpha^2} \quad (30)$$

$$M_5=\left[8.033(A_{11}+A_{22})+5.356\left(A_{12}+2A_{66}\right)\right]\frac{1}{\alpha^2} \quad (31)$$

$$C_1=\left[\left(1.659+1.453\ln\alpha\right)\left(D_{11}+D_{22}\right)+\right.$$
$$\left.+\left(-4.062+0.969\ln\alpha\right)D_{12}+\left(7.379+1.938\ln\alpha\right)D_{66}\right]\frac{1}{\alpha^2} \quad (32)$$

$$C_2=\left[\left(1114.758+36.335\ln\alpha\right)\left(D_{11}+D_{22}\right)+\left(613.985+\right.\right. \quad (33)$$
$$\left.\left.+24.224\ln\alpha\right)D_{12}+\left(1615.549+48.447\ln\alpha\right)D_{66}\right]\frac{1}{\alpha^2}$$

$$C_3=\left[-5.826\left(D_{11}+D_{22}\right)-55.56D_{12}+43.908D_{66}\right]\frac{1}{\alpha^2} \quad (34)$$

For *i*=2, considering only the membrane components of strain energy, *P* is calculated from expressions (26) and (27) where M_{xy} and all C_i terms are now equal to zero.

For *i*=3, considering both bending and membrane components of strain energy we obtain the following (3x3) non-linear system of algebraic equations, from which λ_1, λ_2 and λ_3 can be determined for spe-

cific values of load P:

$$\begin{aligned} P = {} & 2N_1\lambda_1 - N_3\lambda_2 - N_6\lambda_3 + 4M_1\lambda_1^3 - M_5\lambda_2^3 - \\ & - M_{11}\lambda_3^3 + 2M_3\lambda_1\lambda_2^2 - 3M_4\lambda_1^2\lambda_2 + \\ & + 2M_7\lambda_1\lambda_3^2 - 3M_{12}\lambda_1^2\lambda_3 - M_{15}\lambda_2\lambda_3^2 + M_{13}\lambda_2^2\lambda_3 - \\ & - 2M_{14}\lambda_1\lambda_2\lambda_3 + 4M_{xy} + 2C_1\lambda_1 + C_3\lambda_2 + C_6\lambda_3 \end{aligned} \quad (35)$$

$$\begin{aligned} P = {} & -N_3\lambda_1 + 2N_2\lambda_2 - N_5\lambda_3 - M_4\lambda_1^3 + \\ & + 4M_2\lambda_2^3 - M_{10}\lambda_3^3 - 3M_5\lambda_1\lambda_2^2 + 2M_3\lambda_1^2\lambda_2 - \\ & - M_{15}\lambda_1\lambda_3^2 - M_{14}\lambda_1^2\lambda_3 + 2M_8\lambda_2\lambda_3^2 - 3M_9\lambda_2^2\lambda_3 + \\ & + 2M_{13}\lambda_1\lambda_2\lambda_3 + 4M_{xy} + C_3\lambda_1 + 2C_2\lambda_2 + C_5\lambda_3 \end{aligned} \quad (36)$$

$$\begin{aligned} P = {} & -N_6\lambda_1 - N_5\lambda_2 + 2N_4\lambda_3 - M_{12}\lambda_1^3 - M_9\lambda_2^3 + \\ & + 4M_6\lambda_3^3 + M_{13}\lambda_1\lambda_2^2 - M_{14}\lambda_1^2\lambda_2 - \\ & - 3M_{11}\lambda_1\lambda_3^2 + 2M_7\lambda_1^2\lambda_3 - 3M_{10}\lambda_2\lambda_3^2 + 2M_8\lambda_2^2\lambda_3 - \\ & - 2M_{15}\lambda_1\lambda_2\lambda_3 + 4M_{xy} + C_6\lambda_1 + C_5\lambda_2 + 2C_4\lambda_3 \end{aligned} \quad (37)$$

where:

$$\begin{aligned} N_4 &= 39.046(N_x + N_y) + 49.715N_{xy}, \\ N_5 &= 0.361(N_x + N_y) + 0.459N_{xy}, \\ N_6 &= 0.141(N_x + N_y) + 0.18N_{xy} \end{aligned} \quad (38)$$

$$M_6 = \left[2191.104(A_{11} + A_{22}) + 1460.737(A_{12} + 2A_{66})\right]\frac{1}{\alpha^2}, \quad M_7 = \left[64.237(A_{11} + A_{22}) + 42.825(A_{12} + 2A_{66})\right]\frac{1}{\alpha^2} \quad (39)$$

$$M_8 = \left[2665.467(A_{11} + A_{22}) + 1776.976(A_{12} + 2A_{66})\right]\frac{1}{\alpha^2}, \quad M_9 = \left[35.223(A_{11} + A_{22}) + 23.482(A_{12} + 2A_{66})\right]\frac{1}{\alpha^2} \quad (40)$$

$$M_{10} = \left[46.016(A_{11} + A_{22}) + 30.678(A_{12} + 2A_{66})\right]\frac{1}{\alpha^2}, \quad M_{11} = \left[16.677(A_{11} + A_{22}) + 11.118(A_{12} + 2A_{66})\right]\frac{1}{\alpha^2} \quad (41)$$

$$M_{12} = \left[0.378(A_{11} + A_{22}) + 0.252(A_{12} + 2A_{66})\right]\frac{1}{\alpha^2}, \quad M_{13} = \left[168.625(A_{11} + A_{22}) + 112.416(A_{12} + 2A_{66})\right]\frac{1}{\alpha^2} \quad (42)$$

$$M_{14} = \left[28.253(A_{11} + A_{22}) + 18.835(A_{12} + 2A_{66})\right]\frac{1}{\alpha^2}, \quad M_{15} = \left[55.382(A_{11} + A_{22}) + 36.921(A_{12} + 2A_{66})\right]\frac{1}{\alpha^2} \quad (43)$$

$$\begin{aligned} C_4 = {} & \left[(11744.949 + 117.727\ln\alpha)(D_{11} + D_{22}) + \right. \\ & + (7411.381 + 78.485\ln\alpha)D_{12} + \\ & \left. + (16078.518 + 156.97\ln\alpha)D_{66}\right]\frac{1}{\alpha^2} \end{aligned} \quad (44)$$

$$C_5 = \left[-29.824(D_{11} + D_{22}) - 484.976D_{12} + 425.329D_{66}\right]\frac{1}{\alpha^2} \quad (45)$$

$$C_6 = \left[-12.788(D_{11} + D_{22}) - 101.545D_{12} + 75.967D_{66}\right]\frac{1}{\alpha^2} \quad (46)$$

For i=3, considering only the membrane components of strain energy, P is calculated from expressions (35), (36) and (37) where M_{xy} and all C_i terms are now equal to zero.

It is noted that the singular terms of the integral in equation (17) are calculated in a finite part sense. Singular terms in the strain energy calculation appear also in reference [1].